www.amlett.com, www.vbripress.com/aml, DOI: 10.5185/amlett.2014.amwc.1016 Published online by the VBRI press in 2014

Electrical and microstructural properties of (Cu, Al, In)-doped SnO_2 films deposited by spray pyrolysis

Sibel Gürakar*, Tülay Serin, Necmi Serin

Department of Engineering Physics, Ankara University, Ankara 06100, Turkey

*Corresponding author. Fax: (+90) 312 212 7343; E-mail: sgurakar@eng.ankara.edu.tr

Received: 23 October 2013, Revised: 16 November 2013 and Accepted: 30 November 2013

ABSTRACT

The effect of Cu, Al and In doping on the microstructural and the electrical properties of the SnO_2 films were studied. The undoped, Cu, Al and In (2 at. %) doped SnO_2 films were deposited on the glass substrate by spray pyrolysis from 0.8 M $SnCl_2$–ethanol solution at substrate temperature 400 °C. The microstructural properties of films were investigated by X-ray diffraction (XRD) method. It was determined that the films formed at polycrystalline structure in tetragonal phase and structure was not changed by dopant species. The lattice parameters (a), (c) and crystallite size (D) were determined and obtained in the range of 4.90-4.92 Å, 3.26-3.31 Å and 34-167 Å, respectively. The optical transmittance of thin films was measured and the optical band gap E_g values of the films were obtained in the range of 3.96-4.00 eV, using the Tauc relation. The electrical transport properties of undoped, Cu, Al and In-doped SnO_2 films were investigated by means of conductivity measurements in a temperature range of 120-400 K. The electrical transport mechanism of the undoped, Cu, Al and In-doped SnO_2 films was determined by means of the tunneling model through the back-to-back Schottky barrier and the thermionic field emission model in the temperature range of 120-300 K and 300-400 K, respectively. Copyright © 2014 VBRI press.

Keywords: SnO_2; doping; thin films; electrical transport.

Sibel Gürakar is a Ph.D. student and working as a research and teaching assistant since 2009, in the Department of Engineering Physics, Ankara University, Ankara, Turkey. She received the B.S. and M.S. degrees in engineering physics from Ankara University in 2006 and 2009, respectively. Her major research interests include the growth and characterization of thin films, the electrical conductivity measurement, metal oxide systems, the investigation of electronic properties of heterojunction structures composed of various oxide semiconductors.

Tülay Serin is working as a Professor since 1998, in the Department of Engineering Physics, Ankara University, Ankara, Turkey. She received the B.S., M.S., and Ph.D. degrees in engineering physics from Ankara University in 1977, 1983 and 1988, respectively. Since 1988, 1993, and 1998, she has been employed as an Assistant Professor, Associate Professor, and Professor, respectively. Her major research interests include the growth and characterization of thin films, solar cells, metal oxide systems, the investigation of electronic properties of Schottky and pin diode structures composed of various thin layers such as amorphous silicon, silicon, and germanium.

Necmi Serin is working as a Professor since 1990, in the Department of Engineering Physics, Ankara University, Ankara, Turkey. He received the B.S., M.S., and Ph.D. degrees in engineering physics from Ankara University in 1971, 1973 and 1977, respectively. Since 1981 and 1990, he has been employed as an Associate Professor, respectively. His major research interests include the growth and characterization of thin films, the electrical conductivity measurement, the investigation of electronic properties of Schottky and pin diode structures composed of various thin layers such as amorphous silicon, silicon and germanium.

Introduction

Tin dioxide (SnO_2) has been intensively investigated because of its rich physical properties and large applications in commercial devices. The SnO_2 with a wide-band-gap (E_g =3.6-4.0 eV) **[1-3]** is one of the excellent semiconductors which can be applied to solid state gas sensors, sensing arrays, solar cells, photovoltaic cells, organic light emitting diodes, touch sensitive screens and thin film transistors **[4-10]**. The SnO_2 thin films can be fabricated by a number of techniques such as chemical vapour deposition (CVD), metalorganic deposition, rf sputtering, sol–gel dip coating and spray pyrolysis **[11-16]**. It was clearly established that structural, electronic transport and optical properties of SnO_2 films are very sensitive to preparation method, deposition conditions, dopant atoms and amount of dopant atoms. The spray pyrolysis, among the various deposition techniques, is the well suited for the preparation of doped tin dioxide thin films because of its simple and economic experimental arrangement, ease of adding various doping material, reproducibility, high growth rate and mass production capability for uniform large area coatings, which are desirable for industrial and solar cell applications. In order to change the order of electrical conductivity of SnO_2, the doping with various atoms is an effective way. In previous articles, it was declared that the order of electrical conductivity increased with fluorine, antimony, tungsten and decreased with indium, aluminum, copper, lithium, etc. dopant atoms **[17-24]**. On the other hand, there are only a few publications in order to explain the electrical conduction mechanism in doped SnO_2 up to now **[25-28]**. In this study we aimed to determine the effects of Cu, Al and In atoms, in the constant doping ratio, on the electrical conduction mechanism. In order to realize our goal we planned to prepare SnO_2 films on the glass substrate and measure their electrical conductivity in the temperature range of 120-400 K.

Experimental

Synthesis of materials

The glass substrates were ultrasonically cleaned by keeping in ethanol and in the distilled water, for ten minutes, respectively. Then the glass substrates were dried. The films were deposited on the glass substrates by spray pyrolysis technique. In order to prepare the coating solution, firstly, 2.70 g tin chloride dihydrate [$SnCl_2.2H_2O$, 99.99%, Merck, Germany] was dissolved in 5 ml of hydrochloric acid [HCl, 37%, Merck, Germany] by heating at 90 °C. Then 10 ml of ethanol [C_2H_6O, 99.99%, Merck, Germany] was added in the solution. The concentration of the sprayed solution was 0.8 M. The solution flow rate of 2 ml/min was maintained using air as the carrier gas. The distance between the substrate and nozzle was kept at 37 cm. In the period of spraying, the substrate temperature was kept at 400^{o}C. The temperature was controlled by an electronic temperature controller. In order to prepare the Cu, Al and In-doped films, $CuCl_2$ [99.99%, Merck, Germany], $AlCl_3$ [99.99%, Merck, Germany] and $InCl_3$ [99.99%, Alfa Aesar, Germany] were dissolved in 5 ml of ethanol with the same doping ratio 2 at. % and the solutions were added into the coating solution, respectively.

Characterizations

The microstructure of the SnO_2 films was investigated by means of an Inel-Equinox 1000 diffractometer. The radiation source, the wavelength, and the 2θ scanning range of the diffractometer were Co Kα, 0.179 nm and 20–70^o, respectively. The optical band gap of the films was calculated by means of UV–Vis-NIR transmittance measurements performed with a Shimadzu UV-3600 spectrophotometer. The electrical resistance measurements were performed by two-point probe method as a function of temperature using a Keithley 2420 programmable constant current source in the temperature range 120–400 K. The carrier concentrations in the films were determined by Hall-effect measurements at room temperature (RT).

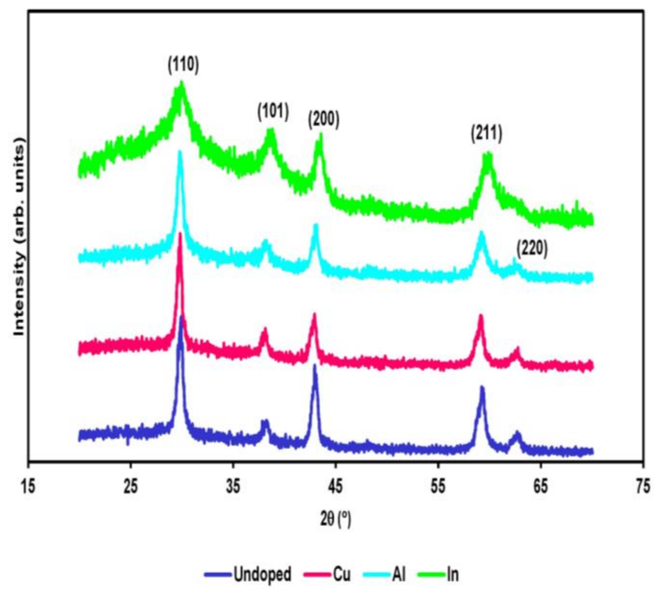

Fig. 1. The XRD patterns recorded for SnO_2 films prepared by various dopant atoms.

Results and discussion

Structural analysis

The XRD patterns of undoped and Cu, Al, In-doped SnO_2 films are shown in **Fig. 1**. The films deposited showed five peaks namely (110), (101), (200), (211) and (220). Since all the peaks are sharp it is evident that the films deposited are polycrystalline in nature and the positions of X-ray diffraction peaks fit well with the tetragonal structure of SnO_2 (JCPDS card tin oxide, 41-1445) **[29]**. As seen from **Fig. 1**, the preferred orientation is (110) plane for undoped SnO_2 film. The addition of Cu, Al and In atoms do not affect the preferred orientation along (110) plane and crystal structure. The dopants do not form extra peaks in the XRD pattern of doped SnO_2 films because dopant atoms incorporate homogeneously into the tin oxide matrix. In the present study, the most conspicuous feature observed in the XRD analysis of the films is orientation along the (110) plane. In literature published on SnO_2 films doped with different atoms such as Al, Zn and Co exhibited similar behaviors **[19, 30]**. This result is consistent with the analysis of the microstructure of undoped SnO_2 films prepared by spray pyrolysis from various solutions by Smith et al. **[31]**. It was seen that the amount of HCl in the starting solution strictly controls the preferred orientation. In the case, the amount of HCl is less than 0.2 mol/l, the preferred orientation occurs as (110). If the amount of HCl is greater than 0.2 mol/l, then the preferred orientation occurs as (101).

The lattice constants a and c for the tetragonal phase structure are determined by the relation **[32]**

$$\frac{1}{d^2}=\left(\frac{h^2}{a^2}+\frac{k^2}{a^2}\right)+\left(\frac{l^2}{c^2}\right) \qquad (1)$$

where d and (hkl) are the interplanar distance and Miller indices, respectively. The calculated lattice constants a, c and c/a values are given in **Table 1**. It was seen that they match well with the Standard JCPDS data card **[29]** and Kulaszewicz's **[33]** results. It was also observed that the various doping atoms did not change the lattice parameters.

Table 1. Lattice parameters and crystallite size values of SnO_2 films prepared for various dopant atoms.

Doping Atom	a (Å)	c (Å)	c/a	D (Å)
Undoped	4.90	3.31	0.68	155
Cu	4.92	3.32	0.68	167
Al	4.90	3.31	0.68	141
In	4.90	3.26	0.67	34

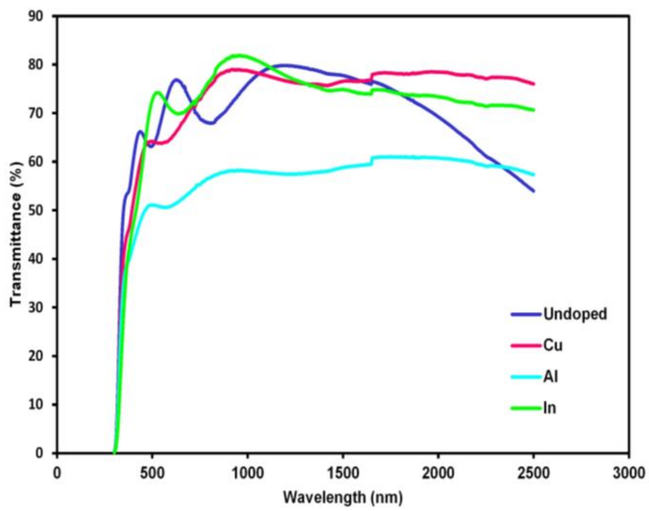

Fig. 2. Transmittance spectra of SnO_2 films prepared by different dopant atoms.

The crystallite size for crystallites with the (110) plane was calculated by Scherrer's formula, $D = 0.9\lambda/(\beta\cos\theta)$ in which the peak broadening due to residual stresses in the films was neglected. Where D, β and λ are the size of the crystallite, the broadening of the diffraction line measured at half its maximum intensity in radians and the wavelength of X-rays (0.179 nm), respectively. The calculated values of crystallite size are listed in **Table 1**. It was observed that the crystallite size of the films depended on the kinds of dopant atoms. This behavior can be explained by means of differences in the ionic radius of Al^{3+}, In^{3+} and Cu^{2+} which the ionic radius of them are 0.050, 0.080 and 0.073 nm, respectively.

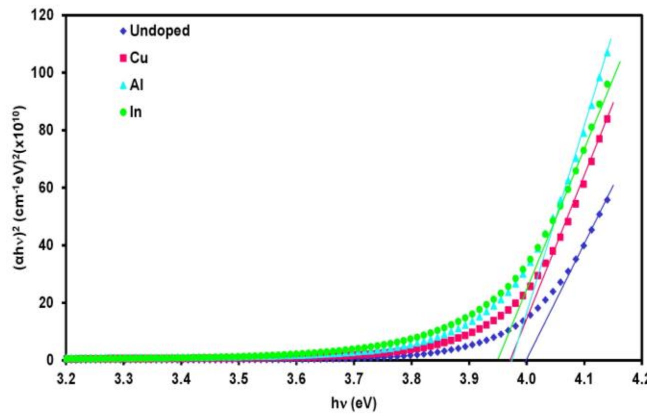

Fig. 3. The variation of $(\alpha h\nu)^2$ versus hν for SnO_2 films for the various dopant atoms.

Optical properties

Fig. 2 shows the optical transmittance spectra of the SnO_2 films for various dopant atoms. The transmittances of all the films were increased in an apparent way with wavelength near the IR region. It was seen that the transmittance has the lowest value for the film doped with Al. The absorption coefficients (α) were determined by means of the optical transmittance spectra using the relation, $\alpha = (1/d)\ln(1/T)$ where d is the thickness and T is the transmittance of the film at a particular wavelength. The optical band gap E_g of the film was calculated using the Tauc relation **[34]**, which is given as $\alpha h\nu=\alpha_0(h\nu-Eg)^n$, where hν, α_0 and n=0.5, 1.5, 2.0 and 3.0 are the photon energy, a constant and for allowed direct, forbidden direct, allowed indirect and forbidden indirect electronic transitions, respectively **[35]**. The plot of $(\alpha h\nu)^2$ versus hν is shown in **Fig. 3.** It was seen that the band-gap energy E_g obeyed to the allowed direct transition (n=1/2) model. The optical energy band gap was obtained by extrapolating the linear portion of $(\alpha h\nu)^2$ versus hν plot to $(\alpha h\nu)^2$=0 as 4.00 eV for undoped, 3.96 eV for In-doped SnO_2 and 3.98 eV for Cu and Al-doped SnO_2 films. The similar values for the optical energy band gaps were also reported by many researches **[1, 2, 36, 37]**.

Electrical measurements

Fig. 4 exhibits the electrical conductivity of undoped and doped SnO_2 films as a function of temperature for the various doping atoms in the temperature range of 120-400K. It was seen that the conductivity for undoped, Al, Cu and In-doped films are almost constant in the temperature range of 120-300 K, but slightly depends on temperature in the temperature range of 300-400 K. It is also observed that the conductivity values significantly depend on the kinds of dopant atom. The electrical conductivity of SnO_2 film decreases with the kinds of dopant atom of Al^{3+}, In^{3+} and Cu^{2+} in all the temperature range. These electrical conductivity behaviors of SnO_2 film can be explained because of the coexistence of donors (intrinsic point defects such as oxygen vacancies and tin interstitials) and acceptors (substitution of Sn^{4+} by In^{3+}, Cu^{2+} or Al^{3+}) in the films and In, Al and Cu atoms behave as acceptors.

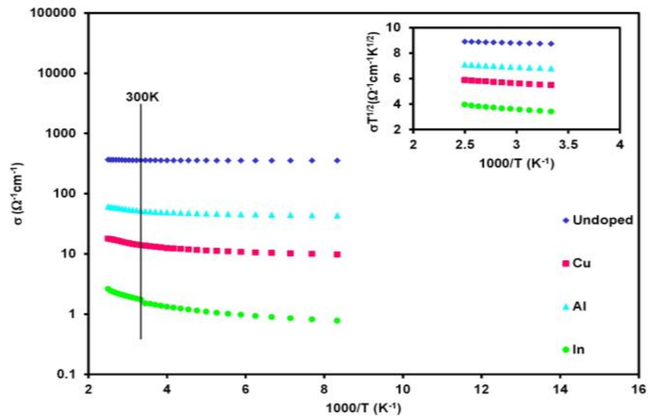

Fig. 4. Conductivity of SnO_2 films as a function of temperature for the various dopant atoms. The inset is the fits of the experimental data for SnO_2 films following Eq. (5).

Orton and Powell **[38]** discussed the band conduction in polycrystalline semiconductors by comparing L with the Debye length L_D [given $L_D=(\varepsilon\varepsilon_0 kT/e^2N)^{1/2}$]. Where, ε, $\varepsilon_{o,}$ k and e are the relative dielectric constant **[39]** of the material given as 12, the dielectric constant of free space, Boltzmann's constant and the electron charge, respectively. The interface trap states create potential barriers in the grain boundary regions in the case $L \geq 2L_D$. It can be said that the flat conduction band occurs. The calculated L_D value for each film is presented in **Table 2**. The grain size values L determined from the atomic force microscopy AFM images. The carrier concentrations N in the films are obtained from Hall effect measurements at the room temperature and the results are also exhibited in **Table 2**. It was observed that all the films have a very low L_D (a few Å) value compared to L. It points out that potential barriers can be created in grain boundary regions when interface traps are present. It should be also noted that the SnO_2 films prepared by the spray pyrolysis technique exhibits large disorders. In other terms, SnO_2 films have a distribution of L, defective grain boundaries, native defects such as oxygen vacancy and extrinsic impurities. It is concluded that a remarkably narrow and low potential barrier is formed at the grain boundary in the case L_D and N are small and high, respectively.

Fig. 5 shows the energy band diagram of back-to-back Schottky barrier **[40]** at a grain boundary for the degenerated films. Three possible transport mechanisms at the grain boundary are illustrated; (i) thermionic emission over the grain boundary, (ii) thermionic field emission and (iii) field emission (direct tunneling) through the grain boundary. For simplicity, the grain is assumed to be a square having a grain size of L cm.

The temperature dependence of the conductivity for undoped, Cu, Al and In-doped SnO_2 films are found constant near RT (120-300 K) **Fig. 4.** The constant conductivity suggests that the tunnel effect plays a major role in the carrier transport across the barrier **[41]**. When it was assumed the potential barrier to be a rectangle of the height V_B and the width l_2, the tunnel current can be easily obtained.

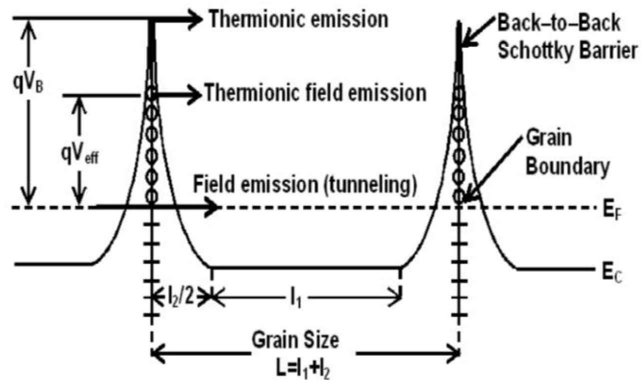

Fig. 5. Energy band diagram and possible carrier transition mechanisms at a grain boundary of the degenerated films.

As to Holm **[42]**, the tunnel current density J_{tun} for a very small applied voltage V across a barrier is given by

$$J_{tun} = \left[q^2V\left(\sqrt{2m^*V_B}\right)/\left(h^2l_2\right)\right]\exp\left[-4\pi l_2\left(\sqrt{2m^*V_B}\right)/h\right] \quad (2)$$

where m* and h are the effective mass of carrier and the Planck constant, respectively. The conductivity by the tunnel effect σ_{tun} becomes

$$\sigma_{tun} = \left[Lq^2\left(\sqrt{2m^*V_B}\right)/\left(h^2l_2\right)\right]\exp\left[-4\pi l_2\left(\sqrt{2m^*V_B}\right)/h\right] \quad (3)$$

This equation indicates that σ_{tun} is proportional to grain size. L, m^*, V_B and l_2 are the unknown quantities and should be determined in Eq. (3). Since L values are given in **Table 2** and for the polycrystalline $SnO_{2,}$ Jousse **[39]** proposes as $m^*=0.15m_0$ where m_0 is the free electron mass. When $Q_t = Nl_2$, $V_B = qQ_t^2/8\varepsilon N$ and equation (3) are solved simultaneously, then V_B and l_2 values can be obtained. The values of Q_t is the gap state density at grain boundaries, V_B and 1_2 are calculated and listed in **Table 2**. It should be noted that all the SnO_2 films satisfy the conditions of $Q_t < NL$ and 1_2 «L. The values of V_B in **Table 2**, compared with those of other polycrystalline materials **[38]** are reasonable.

Table 2. L, N, L_D, V_B, l_2, Q_t and V_{eff} values of SnO_2 films prepared for various dopant atoms.

Doping Atom	L (Å)	N (cm^{-3})	L_D (Å)	V_B (eV)	l_2 (Å)	Q_t (cm^{-2})	V_{eff} (eV)
Undoped	775	1.65×10^{20}	3.23	0.056	14.8	2.00×10^{13}	0.018
Cu	837	5.27×10^{18}	18.10	0.192	27.4	3.71×10^{13}	0.043
Al	707	4.99×10^{19}	5.88	0.132	22.8	3.07×10^{13}	0.032
In	175	1.84×10^{18}	30.60	0.212	28.9	3.90×10^{13}	0.056

Undoped, Cu, Al and In-doped SnO_2 films reveal a weak T-dependent σ behavior beyond RT (300–400 K); σ gradually increases with an increase in T. The gradual increase in σ with T for the undoped and lightly doped degenerate films can be attributed to the influence of the grain boundary scattering. Thermionic emission over grain-boundary is known as the typical grain boundary scattering mechanism for polycrystalline semiconductor films. Based on Maxwell-Boltzmann statistics, a conductivity limited by thermionic emission over the back-to-back Schottky barrier is expressed as **[40]**.

$$\sigma = Lq^2N\left(2\pi m^*kT\right)^{-1/2}\exp\left(-qV_B/kT\right) \tag{4}$$

Thermionic field emission consists of two steps; (i) the thermal activation of trapped or free charges in the grain boundary region and (ii) the subsequent tunneling of the thermally activated charges through the potential barrier as in **Fig. 5 [43]**. The kinetic equation for thermionic field emission through the back-to-back Schottky barrier can be approximated by modifying Eq. (4) to

$$\sigma = BT^{-1/2}\exp\left(-V_{eff}/kT\right) \tag{5}$$

where B is a weakly T-dependent parameter and V_{eff} is the effective barrier height for the thermal emission of electrons to tunneling possible sites **[44]**. The V_{eff} values are also determined from the ln($\sigma T^{1/2}$)-1/T plot in the 300-400 K T region as shown in **Fig. 4** and presented in **Table 2**.

The electrical conduction mechanism of our films was compared with the published results of the other researchers [25-28, 41]. At these references, they dealt with fluorine doped prepared by CVD method, undoped by CVD method, undoped by reactive sputtering, fluorine doped by spray pyrolysis and undoped by CVD, respectively. The electrical conduction mechanism of these SnO_2 films were metallic, Efros-Shklovskii variable range hopping (VRH), VRH, VRH and tunneling, respectively. The temperature range of these studies was about 50-300 K. In our case, it was 120–400 K and the electrical transport mechanism was the tunneling model through the back-to-back Schottky barrier and the thermionic field emission model in the temperature range of 120-300 K and 300-400 K, respectively. It was observed that the transport mechanism did not change with the kinds of dopant atoms.

Conclusion

In this study it was concluded that the kind of dopant atoms did not change the structure of undoped and Cu, Al and In-doped SnO_2 films grown by spray pyrolysis. The orientation of the films was along the (110) plane. The films were polycrystalline in nature and had tetragonal structure. The ratio of lattice parameters (c/a) was found as 0.67. The crystallite size of the films calculated from XRD depending on the kind of dopant atoms. The transmittances of all the films were apparently increased with increasing wavelength near the IR region and the transmittance has the lowest value for the film doped with Al. The forbidden band-gap energy value was found as 4.00 eV and 3.96 eV for undoped and In-doped SnO_2 film, respectively. E_g was determined as 3.98 eV, having the same result for Cu and Al-doped SnO_2 films. The temperature dependence of the electrical conductivity of undoped, Cu, Al and In-doped SnO_2 films is found constant in the temperature range of 120-300 K and changes gradually in the temperature range of 300-400 K. The electrical transport mechanism of the undoped, Cu, Al and In-doped SnO_2 films was determined by means of the tunneling model through the back-to-back Schottky barrier and the thermionic field emission model in the temperature range of 120-300 K and 300-400 K, respectively.

Acknowledgements

This work was supported by the Ankara University BAP under Project number 13H4343001. We would also like to thank Prof. Dr. Yusuf Kağan Kadıoğlu for providing XRD measurements.

Reference

1. Bagheri Mohagheghi, M. M.; Shahtahmasebi, N.; Alinejad, M.R.; Youssefi, A.; Shokooh Saremi, M. *Physica B*. **2008,** *403*, 2431–2437.
   DOI: 10.1016/j.physb.2008.01.004
2. Khan, A. F.; Mehmood, M.; Aslam, M.; Ashraf, M. *Applied Surface Science*. **2010,** *256*, 2252–2258.
   DOI: 10.1016/j.apsusc.2009.10.047
3. Moharrami, F.; Bagheri Mohagheghi, M. M.; Azimi Juybari, H. *Thin Solid Films*. **2012,** *520*, 6503–6509.
   DOI: 10.1016/j.tsf.2012.06.075
4. Rani, S.; Roy, S. C.; Bhatnagar, M.C. *Sensors and Actuators B*. **2007,** *122*, 204–210.
   DOI: 10.1016/j.snb.2006.05.032
5. Maekava, T.; Suzuki, K.; Takada, T.; Kobayashi, T.; Egashira, M. *Sensors and Actuators B.* **2001,** *80*, 51-58.
   DOI: 10.1016/S0925-4005(01)00885-1
6. Agashe, C.; Hüpkes, J.; Schöpe, G.; Berginski, M. *Solar Energy Materials & Solar Cells*. **2009,** *93*, 1256–1262.
   DOI: 10.1016/j.solmat.2009.01.021
7. Yin, L. T.; Chou, J. C.; Chung, W. Y.; Sun, T. P.; Hsiung, S.-K. *Sensors and Actuators B*. **2000,** *71*, 106-111.
   DOI: 10.1016/S0925-4005(00)00613-4
8. Ouerfelli, J.; Djobo, S. Ouro.; Bernède, J.C.; Cattin, L.; Morsli, M.; Berredjem, Y. *Materials Chemistry and Physics.* **2008,** *112*, 198–201.
   DOI: 10.1016/j.matchemphys.2008.05.029
9. Kikuchi, N.; Kusano, E.; Kishio, E.; Kinbara, A. *Vacuum*. **2002,** *66*, 365–371.
   DOI: 10.1016/S0042-207X(02)00156-2
10. Kim, W. J.; Koo, W. H.; Jo, S. J.; Kim, C. S.; Baik, H. K.; Lee, J.; Im, S. *Applied Surface Science*. **2005,** *252*, 1332–1338.
    DOI: 10.1016/j.apsusc.2005.02.100
11. Fang, T. H.; Chang, W. J. *Applied Surface Science.* **2003,** *220*, 175–180.
    DOI: 10.1016/S0169-4332(03)00817-1
12. Dippel, A. C.; Schneller, T.; Gerber, P.; Waser, R. *Thin Solid Films.* **2007,** *515*, 3797–3801.
    DOI: 10.1016/j.tsf.2006.09.045
13. Ma, J.; Hao, X.; Huang, S.; Huang, J.; Yang, Y.; Ma, H. *Applied Surface Science*. **2003,** *214*, 208–213.
    DOI: 10.1016/S0169-4332(03)00344-1
14. Gasparro, G.; Pütz, J.; Ganz, D.; Aegerter, M. A. *Solar Energy Materials and Solar Cells.* **1998,** *54*, 287-296.
    DOI: 10.1016/S0927-0248(98)00080-4
15. Elangovan, E.; Ramesh, K.; Ramamurthi, K. *Solid State Communications.* **2004,** *130*, 523–527.
    DOI: 10.1016/j.ssc.2004.03.015
16. Serin, T.; Serin, N.; Karadeniz, S.; Sarı, H.; Tuğluoğlu, N.; Pakma, O. *Journal of Non-Crystalline Solids*. **2006,** *352*, 209–215.
    DOI: 10.1016/j.jnoncrysol.2005.11.031
17. Alsac, A. A.; Yildiz, A.; Serin, T.; Serin, N. *J. Appl. Phys*. **2013,** *113*, 063701.
    DOI: 10.1063/1.4790879
18. Miao, D.; Zhao, Q.; Wu, S.; Wang, Z.; Zhang, X.; Zhao, X.; *Journal of Non-Crystalline Solids.* **2010,** *356*, 2557–2561.
    DOI: 10.1016/j.jnoncrysol.2010.06.076
19. Ahmed, Sk. F.; Khan, S.; Ghosh, P. K.; Mitra, M. K.; Chattopadhyay, K. K. *J Sol-Gel Sci Techn.* **2006,** *39*, 241–247.
    DOI: 10.1007/s10971-006-7808-x

20. Patil, S. B.; Patil, P. P.; More, M. A. *Sensors and Actuators B.* **2007,** *125*, 126–130.
DOI: 10.1016/j.snb.2007.01.047
21. Safonova, O. V.; Rumyantseva, M. N.; Ryabova, L. I.; Labeau, M.; Delabouglise, G.; Gaskov, A. M. *Materials Science and Engineering B.* **2001,** *85*, 43–49.
DOI: 10.1016/S0921-5107(01)00640-7
22. Joseph, D. P.; Renugambal, P.; Saravanan, M.; Raja, S. P.; Venkateswaran, C. *Thin Solid Films.* **2009,** *517*, 6129–6136.
DOI: 10.1016/j.tsf.2009.04.047
23. Manoj, P.K.; Joseph, B.; Vaidyan, V.K.; Amma, D.S.D. *Ceramics International.* **2007,** *33*, 273–278.
DOI: 10.1016/j.ceramint.2005.09.016
24. Huang, Y.; Li, G.; Feng, J.; Zhang, Q. *Thin Solid Films.* **2010,** *518*, 1892–1896.
DOI: 10.1016/j.tsf.2009.07.119
25. Gao, K. H.; Lin, T.; Liu, X. D.; Zhang, X. H.; Li, X. N.; Wu, J.; Liu, Y. F.; Wang, X. F.; Chen, Y. W.; Ni, B.; Dai, N.; Chu, J. H. *Solid State Communications*. **2013,** *157*, 49–53.
DOI: 10.1016/j.ssc.2012.12.024
26. Ma, Y. J.; Zhou, F.; Lu, L.; Zhang, Z. *Solid State Communications.* **2004,** *130*, 313–316.
DOI: 10.1016/j.ssc.2004.02.013
27. Bansal, S.; Pandya, D. K.; Kashyap, S. C. *Thin Solid Films.* **2012,** *524*, 30–34.
DOI: 10.1016/j.tsf.2012.09.062
28. Ramaiah, K. S.; Raja, V. S. *Applied Surface Science.* **2006,** *253*, 1451–1458.
DOI: 10.1016/j.apsusc.2006.02.019
29. JCPDS Powder Diffraction File card 41–1445.
30. Vijayalakshmi, S.; Venkataraj, S.; Subramanian, M.; Jayavel, R. *J. Phys. D: Appl. Phys.* **2008,** *41*, 035505 (7pp).
DOI: 10.1088/0022-3727/41/3/035505
31. Smith, A.; Laurent, J. M.; Smith, D. S.; Bonnet, J. P.; Clemente, R. R. *Thin Solid Films.* **1995,** *266*, 20-30.
DOI: 10.1016/0040-6090(95)06648-9
32. Cullity, B. D. *Elements of X-Ray Diffraction*, 2nd ed. Addison-Wesley Publishing Company: London, **1978,** 555.
33. Kulaszewicz, S. *Thin Solid Films.* **1980,** *74*, 211-218.
DOI: 10.1016/0040-6090(80)90083-8
34. Tauc, J. C. *Optical Properties of Solids.* North-Holland Publ. Amsterdam, **1972**, 279.
35. Tauc, J. C.; Menth, A. *J. Non-Cryst. Solids.* **1972,** *8*, 569.
DOI: 10.1016/0022-3093(72)90194-9
36. Benouis, C. E.; Benhaliliba, M.; Yakuphanoglu, F.; Silver, A. T.; Aida, M. S.; Juarez, A. S. *Synthetic Metals.* **2011,** *161*, 1509–1516.
DOI: 10.1016/j.synthmet.2011.04.017
37. Bagheri Mohagheghi, M. M.; Shokooh Saremi, M. *J. Phys. D: Appl. Phys.* **2004,** *37*, 1248–1253.
DOI: 10.1088/0022-3727/37/8/014
38. Orton, J. W.; Powell, M. J. *Rep. Prog. Phys.* **1980,** *43*, 1263.
DOI: 10.1088/0034-4885/43/11/001
39. Jousse, D. *Phys. Rev. B.* **1985,** *31*, 5335–5342.
DOI: 10.1103/PhysRevB.31.5335
40. Seto, J. Y. W. *J. Appl. Phys.* **1975,** *46*, 5247.
DOI: 10.1063/1.321593
41. Kojima, M.; Kato, H.; Imai, A.; Yoshida, A. *J. Appl. Phys.* **1988,** *64*, 1902.
DOI: 10.1063/1.341741
42. Holm, R. *J. Appl. Phys.* **1951,** *22*, 569.
DOI: 10.1063/1.1700008
43. De Groot, A. W.; McGonigal, G. C.; Thomson, D. J.; Card, H. C. *J. Appl. Phys.* **1984,** *55*, 312.
DOI: 10.1063/1.333099
44. Tarng, M. L. *J. Appl. Phys.* **1978,** *49*, 4069.
DOI: 10.1063/1.325367